Flexibility of Integrated Power and Gas Systems: Modeling and Solution Choices Matter

Online Companion

Enrica Raheli, Yannick Werner, Jalal Kazempour

This document is an online companion (OC) for the paper "Flexibility of Integrated Power and Gas Systems: Modeling and Solution Choices Matter". Numbered sections and equations throughout the online companion correspond to those in the paper, while the prefix 'OC.' denotes these elements within this document.

Section OC.1 shows how Euler's equations governing the gas flow are simplified for high-pressure transmission pipelines. In Section OC.2, we discuss the impact of modeling choices on the gas flow problem. Section OC.3 introduces the full mathematical formulation of the optimal power and gas flow problem. Section OC.4 provides additional details on the solution approaches described in Section IV of the main paper. In Section OC.5, we propose a per-unit conversion of the optimal power-gas flow problem. Finally, in Section OC.6, we show the large-scale integrated power and gas network, i.e., Case Study B, together with a short analysis.

OC.1. Original gas flow equations

The one-dimensional dynamic flow of natural gas along the pipeline axis is governed by a set of nonlinear and nonconvex PDEs, named Euler's equations (A.1)-(A.3) [1]:

$$\frac{\partial \rho}{\partial t} + \frac{\partial (\rho u)}{\partial x} = 0 \tag{A.1}$$

$$\frac{\partial (\rho u)}{\partial t} + \frac{\partial \pi}{\partial x} + \frac{\partial (\rho u^2)}{\partial x} + \rho g \sin\alpha + \lambda \frac{\rho u |u|}{2D} = 0 \tag{A.2}$$

$$\frac{\partial}{\partial t}\left[\rho\left(e + \frac{1}{2}u^2\right)\right] + \frac{\partial}{\partial x}\left[(\rho u)\left(h + \frac{1}{2}u^2\right)\right] - \rho\Omega + \rho g u \sin\alpha = 0, \tag{A.3}$$

where t and x represent the time and space dimensions. The symbols ρ, u, and π describe the density, velocity, and pressure of the natural gas, respectively. Pipeline-specific constants D, α, and λ denote the diameter, inclination angle, and friction factor[1] of the pipeline's inner walls. Constant g denotes the acceleration of gravity. The symbols e and h represent the specific internal energy

[1] The friction factor is a function of the pipeline characteristics (i.e., diameter, roughness, and Reynolds number). For natural gas transmission pipelines, it can be calculated with the Colebrook-White equation for turbulent flow since the Reynolds number of the gas is high enough [2].

and enthalpy of the gas, respectively, whereas Ω is the heat transfer rate per unit of time and mass. The continuity equation (A.1) describes the principle of conservation of mass in a differential form, stating that the net mass rate flowing outside a differential gas volume is equal to the rate of decrease in the mass present within the differential volume [3]. The conservation of momentum equation (A.2) represents the differential form of Newton's second law, stating that, at each time instant, the sum of all forces exerted on a fluid volume is equal to the rate of increase in momentum. The forces appearing in equation (A.2) are: the natural gas *inertia term* $\frac{\partial(\rho u)}{\partial t}$, the *pressure gradient* along the axis $\frac{\partial \pi}{\partial x}$, the advection $\frac{\partial(\rho u^2)}{\partial x}$, the force of gravity $\rho g \sin\alpha$, and the *friction force* $\lambda \frac{\rho u|u|}{2D}$. Finally, (A.3) enforces energy conservation in differential form. In addition to those three PDEs, the equation of state relates the gas state variables (i.e., density, pressure, and temperature):

$$\pi = \frac{Z(\pi, T) R T}{M_g} \rho, \tag{A.4}$$

where Z is the natural gas compressibility factor, which is a function of pressure and temperature, R is the universal gas constant, T is the absolute temperature, and M_g is the molecular weight of natural gas.

For high-pressure natural gas transmission pipelines, the following three assumptions are generally adopted to simplify Equations (A.1)–(A.4):

1. In (A.2), the advection term $\frac{\partial(\rho u^2)}{\partial x}$ and the impact of non-horizontal pipelines $\rho g \sin\alpha$ are negligible compared to the pressure gradient $\frac{\partial \pi}{\partial x}$ [3, 4], and therefore dropped.
2. Flow is assumed to be isothermal, meaning the temperature is constant and the pipeline is in thermal equilibrium with the environment ($\Omega = 0$) [3–5]. Consequently, (A.3) can be neglected.
3. In (A.4), the compressibility factor is assumed to be constant in both temperature (following the isothermal flow assumption) and pressure. This implies a direct proportionality between gas pressure and density, which simplifies (A.4) to $\pi = c^2 \rho$, where c is the speed of sound in gas and is defined as $c^2 = \frac{ZRT}{M_g}$.

By using the cross-sectional pipeline area A, introducing the mass flow $m = \rho u A$, and applying the simplifying assumptions above, (A.1)-(A.4) can be rewritten as:

$$\frac{\partial \pi}{\partial t} + \frac{c^2}{A} \frac{\partial m}{\partial x} = 0 \tag{A.5}$$

$$\underbrace{\frac{\partial m}{\partial t}}_{\text{Inertia term}} + \underbrace{A \frac{\partial \pi}{\partial x}}_{\text{Pressure gradient}} + \underbrace{\frac{\lambda c^2}{2DA} \frac{m|m|}{\pi}}_{\text{Friction force}} = 0. \tag{A.6}$$

OC.2. Gas flow problem: Impact of modeling choices

In this section, we assess the impact of modeling choices on the optimal gas flow problem. Similarly to [6], we do not take a power system perspective but focus on gas network state variables. Therefore, we do not solve the integrated optimal power-gas flow problem, but only the optimal gas flow

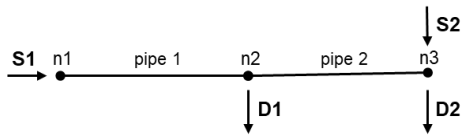

Figure OC.1 Schematic representation of the 3-node natural gas network.

problem. This consists in minimizing objective function (B.1) without power system costs, subject to the gas system constraints (B.4a)- (B.7). A stylized 3-node natural gas transmission network is used as an illustrative case study. The network topology is shown in Figure OC.1, and all the parameters are reported in the Github repository [7]. The simplifying assumptions introduced to obtain the ST and QD models are challenged when the gas load changes rapidly (i.e., the temporal derivatives in (2)-(3) give a significant contribution). Therefore, we analyze an extreme scenario where the gas load at node 2 is linearly increased from 10% to 100% over 30 minutes, representing, for instance, the sudden ramp-up of a very large gas-fired peak power plant. Considering an efficiency of 30% and a gas lower heating value of 13.6 kWh/kg, the power plant size is 1469 MW. The load at node 3 is kept constant during the 5-hour time horizon. Before the ramp-up starts at hour 3:00, the cheaper gas source S1 is able to cover both loads. The more expensive source S2 (which could for example represent a large underground storage facility) is activated to meet the increasing load, resulting in a change of flow direction for pipeline 2. The load input data are provided every 5 minutes, and the optimization problem is solved with the commercial nonlinear solver Ipopt.

OC.2.1. Impact of discretization

First, the impact of space and time discretization is analyzed. For the ST model, having a more refined discretization in space does not give an additional contribution, since the mass flow is assumed to be constant along the pipe, as explained in Section III-C. Having a more refined discretization in time gives a contribution only if the load input data are available with a granularity smaller than the chosen time step (e.g., the load data are available every 15 minutes, and a 1-hour time step is adopted). By choosing a coarser discretization (e.g., 1-hour) and performing the average, the peaks in the load profile are smoothed out. However, if the load input data are provided only every hour, refining the time discretization and assuming that the load is constant over the whole hour does not affect the solution of the steady-state model.

Conversely, for the QD and DY models, we observe that the space and time discretization have a significant impact on the optimal solution since they directly affect the way the original PDEs are approximated. This is often neglected in the literature about integrated power-gas systems, where generally a 1-hour time step and no space discretization (i.e., in each pipeline, Δx equal to

its length) are adopted [8–12], without assessing the solution quality. We focus here on the QD model, but the presented results similarly apply to the DY model. The solution obtained with our most refined discretization in space and time chosen here, $\Delta x = 5$ km and $\Delta t = 300$ s, is used as a reference to compare the impact of a coarser mesh.

In Fig. OC.2a, the impact of space discretization on the pressure values at node 3 is shown: Δx is gradually increased by keeping Δt constant and equal to the reference. For $\Delta x = 100$ km, equal to the length of the pipelines, a maximum relative error of -4.9% with respect to the reference is observed. By only discretizing each pipeline in two segments (i.e., $\Delta x = 50$ km) the maximum relative error is reduced to -0.8%. Similarly, in Fig. OC.2b, the impact of time discretization is assessed. By choosing a 1-hour time-step, a maximum relative error of 13.1% is observed, while with 15 minutes, this is significantly reduced to 1.4%. Improving the temporal discretization has a bigger impact on the solution accuracy than improving the spatial discretization. The reason is that the finite difference method used to discretize the original PDEs is characterized by a first order error in time, and second order error in space (i.e., the error decreases linearly with Δt and quadratically with Δx) [6, 13]. Finally, in Fig. OC.2c, the combined impact of both space and time discretizations is assessed, comparing the most refined reference discretization, with an intermediate discretization ($\Delta x = 50$ km and $\Delta t = 900$ s), and the very coarse discretization that is often adopted in the literature (1-hour time discretization, and no space discretization). In Fig. OC.2, the pressure at node 3 is used to illustrate the impact of discretization, but significant relative errors are observed also on the values of the other optimal variables, such as pipeline inflow and outflow, dispatch decisions, and linepack estimation. The latter especially is critical when assessing the flexibility provided by the natural gas network to the power system. Since the linepack value is proportional to the average pressure in the pipe, as shown by (9), a significant error in the pressure at the nodes can result in an overestimation or underestimation of the linepack potential. In the analyzed case study, the relative error on the linepack value of pipeline 2 reaches 8.6% in one of the time instants when the most coarse discretization is adopted (1-hour time discretization, and no space discretization), and only 0.8% if we choose the intermediate discretization ($\Delta x = 50$ km and $\Delta t = 900$ s). The discretization, especially the temporal one, should therefore be carefully selected when modeling the integrated operation of the power-gas system to avoid an overestimation of linepack flexibility. The day-ahead scheduling for power systems is generally solved with a 1-hour time step, but using the same discretization for the gas problem could lead to significant errors in the flexibility estimation.

OC.2.2. DY **vs.** QD **vs.** ST

The ST model is not suitable to assess the flexibility provided by the gas network to the power system since it does not capture linepack flexibility. Moreover, adopting the ST model for describing

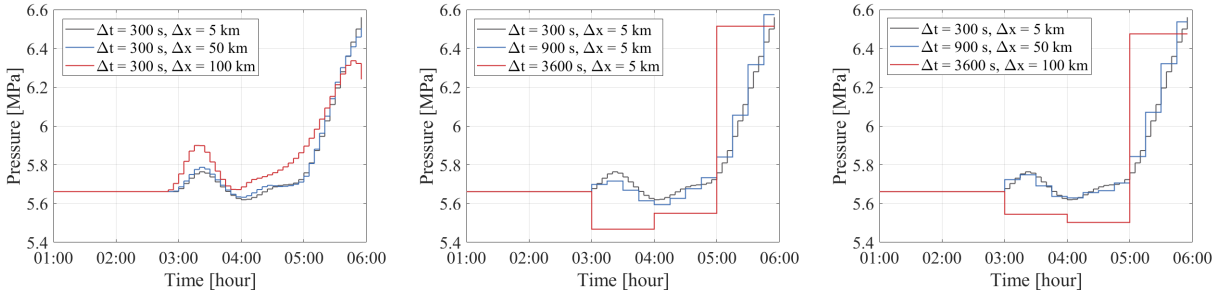

Figure OC.2 **Pressure at node 3 for the quasi-dynamic model. (a) Impact of space discretization. (b) Impact of time discretization. (c) Combined impact of space and time discretization.**

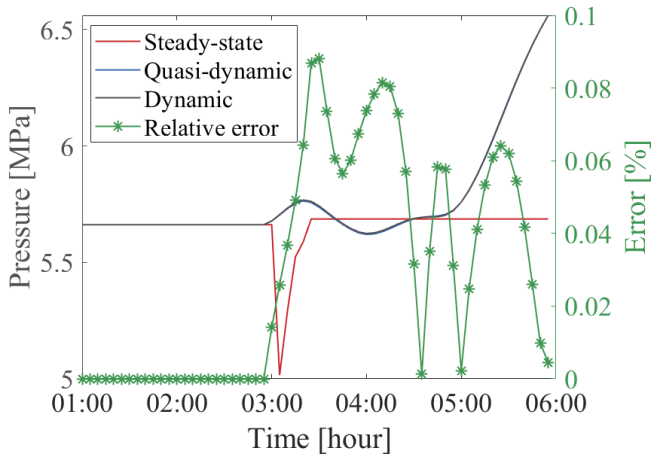

Figure OC.3 **Left axis: pressure at node 3 for the steady-state ($\Delta x = 100$ km and $\Delta t = 300$), quasi-dynamic ($\Delta x = 5$ km and $\Delta t = 300$), and dynamic model ($\Delta x = 5$ km and $\Delta t = 300$). Right axis: relative error between the quasi-dynamic and dynamic model.**

the short-term operation of natural gas networks can lead to infeasible and sub-optimal solutions for real-time operation. We hypothesize that the ST model could be adequate for long-term planning problems, but the error introduced by neglecting the linepack on the investment decisions should be further assessed and is out of the scope of this paper. It has to be reminded that, for the ST model, refining the spacial discretization does not improve the solution accuracy, therefore Δx equal to the length of the pipeline is always adopted in this analysis. Fig. OC.3 shows the pressure profile at node 3 for the ST, QD and DY models with our most refined discretization. Since the QD and DY profile overlap almost perfectly, the right y-axis of Fig. OC.3 shows the relative error between the two models (considering the DY model as a reference). For all time-steps, the relative error is lower than 0.1%. The relative error is even lower if a coarser time discretization is adopted.

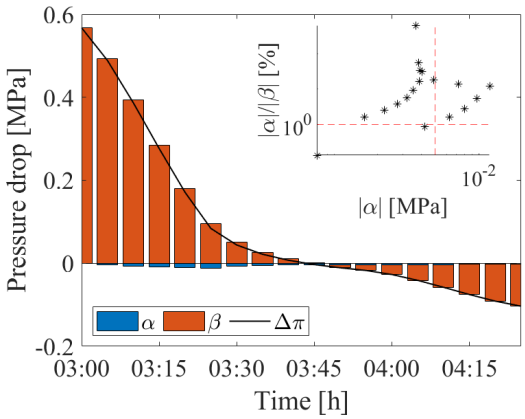

Figure OC.4 **Pressure drop in pipeline 2 from hour 3:00 to hour 4.30: contribution of the inertia and friction terms. The inset plot shows the absolute and relative contribution of the inertia term in pipeline 2 compared to the defined thresholds.**

As already highlighted in Section III-B, the QD model is obtained by neglecting the inertia term (i.e., the temporal derivative) in the momentum equation. By rearranging (5), we express the pressure drop in each pipeline (or sub-pipeline) as [14]:

$$\pi_{i,t} - \pi_{j,t} = \underbrace{\frac{\Delta x}{A}\frac{m_{ij,t} - m_{ij,t-1}}{\Delta t}}_{\alpha} + \underbrace{\frac{\Delta x}{A}\frac{\lambda c^2}{2DA}\frac{m_{ij,t}|m_{ij,t}|}{\pi_{ij,t}}}_{\beta}, \tag{A.7}$$

where α represents the contribution of the inertia term to the total pressure drop, and β is the contribution of the friction with the inner pipeline walls. Since the pressure drop is the sum of the inertia and friction contributions, the QD model is a satisfactory approximation of the DY model when the value of α is small (in both absolute and relative terms). In realistic operating conditions, the inertia term can be considered negligible when $|\alpha| < 50\,\text{Pa/km}$ and $|\alpha|/|\beta| < 1\%$ [14].

In our case study, due to the very fast ramp up of the load in node 2, the thresholds are shortly exceeded in pipeline 2, where the change in flow direction occurs. This is shown is Fig. OC.4, where the pressure drop contributions are plotted from hour 3:00 to hour 4:30. The plot inset in Fig. OC.4 depicts the absolute and relative contribution of α in pipeline 2 compared to the defined thresholds. During the fast ramp up, the thresholds are both violated during only 5 time-steps (out of 60). When the flow approaches zero (before changing direction) and β is almost zero, the relative contribution of α is not negligible, but the absolute threshold is not violated. In pipeline 1, despite the very fast ramp-up occurring, both the absolute and relative thresholds for α are never violated.

Even in the very extreme case study considered, the thresholds are only shortly violated. If a bigger discretization time-step is selected, the impact of the inertia term would be even smaller. In

accordance with what is found in [14–16], the QD model is suitable to be used for the scheduling phase while the dynamic model has to be adopted in real-time to ensure feasibility (similarly to the power system, where DC OPF is used for scheduling, while AC OPF is then adopted for real-time operation). Improving the discretization (especially the time discretization) has a bigger impact on solution accuracy than including the inertia term.

OC.3. Optimal power and gas flow

In the following, we introduce the full formulation of the optimal power-gas flow problem (1). Let $t \in \mathcal{T}$ denote the set of time steps. For the gas network, sets $\mathcal{S}$, $\mathcal{D}$, $\mathcal{P}$, $\mathcal{C}$ represent gas suppliers, gas loads, pipelines, and compressors, respectively. Gas nodes are indicated by $i, j \in \mathcal{I}$. For the power system, $\mathcal{K}$, $\mathcal{G} \subseteq \mathcal{K}$, $\mathcal{W}$, $\mathcal{R}$, $\mathcal{L}$, denote dispatchable generators, GFPPs, wind farms, electrical loads, and lines. Power buses are represented by $n, m \in \mathcal{N}$. The sets $\Psi_i^{(\cdot)}$ and $\Psi_n^{(\cdot)}$ denote, respectively, the assets located at gas network i and at power bus n. Gas nodes connected to node i and power buses connected to bus n are denoted by Ω_i and Ω_n, respectively.

OC.3.1. Objective function

The objective function (B.1) minimizes the total system operating cost over the time steps t of length Δt, as the sum of gas supplies $q^{\mathrm{S}}_{s,t}$ and power generation $p_{k,t}$ from non-GFPPs. Quadratic cost functions are assumed for gas suppliers s and generators.[2] Gas and electrical load shedding, i.e., $q^{\mathrm{O}}_{d,t}$ and $p^{\mathrm{O}}_{r,t}$, are allowed at the prices $C^{\mathrm{sh,G}}$ and $C^{\mathrm{sh,P}}$, respectively.

$$\begin{aligned}\min_{\mathbf{w},\mathbf{v},\mathbf{x},\mathbf{y}} \quad & \frac{\Delta t}{3600} \sum_{t\in\mathcal{T}} \Bigg[\sum_{s\in\mathcal{S}} (A^{\mathrm{Q}}_s (q^{\mathrm{S}}_{s,t})^2 + A^{\mathrm{L}}_s q^{\mathrm{S}}_{s,t}) + \sum_{d\in\mathcal{D}} C^{\mathrm{sh,G}} q^{\mathrm{O}}_{d,t} \\ & + \sum_{k\in(\mathcal{K}\setminus\mathcal{G})} (A^{\mathrm{Q}}_k p^2_{k,t} + A^{\mathrm{L}}_k p_{k,t}) + \sum_{r\in\mathcal{R}} C^{\mathrm{sh,P}} p^{\mathrm{O}}_{r,t} \Bigg].\end{aligned} \tag{B.1}$$

OC.3.2. Power system constraints

The power system constraints are enforced for each time step $t \in \mathcal{T}$ as follows:

$$\underline{P}_k \le p^{\mathrm{G}}_{k,t} \le \overline{P}_k, \qquad \forall\, k \in \mathcal{K}, \tag{B.2a}$$

$$0 \le p^{\mathrm{W}}_{w,t} \le P^{\mathrm{W}}_{w,t}, \qquad \forall\, w \in \mathcal{W}, \tag{B.2b}$$

$$0 \le p^{\mathrm{O}}_{r,t} \le P^{\mathrm{D}}_{r,t}, \qquad \forall\, r \in \mathcal{R}, \tag{B.2c}$$

$$f_{nm,t} = B_{nm}(\theta_{n,t} - \theta_{m,t}), \qquad \forall\, (n,m) \in \mathcal{L}, \tag{B.2d}$$

$$-F_{nm} \le f_{nm,t} \le F_{nm}, \qquad \forall\, (n,m) \in \mathcal{L}, \tag{B.2e}$$

$$\theta_{n,t} = 0, \qquad n = n^{\mathrm{ref}}, \tag{B.2f}$$

[2] For power, the linear A^{L}_k and quadratic A^{Q}_k cost coefficients are, respectively, in €/(MW h) and €/(MW^2 h). For gas, A^{L}_s and A^{Q}_s are in €s/(kg h) and €s^2/(kg^2 h).

$$\sum_{k\in\Psi_n^{\mathcal{K}}} p_{k,t}^{\mathrm{G}} + \sum_{w\in\Psi_n^{\mathcal{W}}} p_{w,t}^{\mathrm{W}} - \sum_{m\in\Omega_n} f_{nm,t} - \sum_{r\in\Psi_n^{\mathcal{R}}} (P_{r,t}^{D} - p_{r,t}^{\mathrm{O}}) = 0, \qquad \forall\, n\in\mathcal{N}. \tag{B.3}$$

Constraint (B.2a) ensures that dispatchable generators operate between their minimum and maximum limits, $\underline{P}_k$ and $\overline{P}_k$. In (B.2b), the wind dispatch $p_{w,t}^{\mathrm{W}}$ is upper bounded by the forecasted wind production $P_{w,t}^{\mathrm{W}}$. Constraint (B.2c) states that electrical load shedding should not exceed the electrical load $P_{r,t}^{\mathrm{D}}$. Constraint (B.2d) is the DC power flow approximation, where $f_{nm,t}$ is the line power flow, $\theta_{n,t}$ and $\theta_{m,t}$ the nodal voltage angels, and B_{nm} is the line susceptance. Constraint (B.2f) enforces the power flow to be within the line capacity limit F_{nm}. Constraint (B.2f) defines the reference voltage bus. Finally, (B.3) ensures the nodal power balance between generation and demand.

OC.3.3. Gas system constraints

The gas system constraints are enforced for each time step $t\in\mathcal{T}$ as follows:

$$\underline{Q}_s \le q_{s,t}^{\mathrm{S}} \le \overline{Q}_s, \qquad \forall\, s\in\mathcal{S}, \tag{B.4a}$$

$$\underline{\Pi}_i \le \pi_{i,t} \le \overline{\Pi}_i, \qquad \forall\, i\in\mathcal{I}, \tag{B.4b}$$

$$\pi_{i,t} = \Pi_i^{\mathrm{S}}, \qquad \forall\, i\in\mathcal{I}^{\mathrm{S}}, \tag{B.4c}$$

$$0 \le q_{d,t}^{\mathrm{O}} \le Q_{d,t}^{\mathrm{D}}, \qquad \forall\, d\in\mathcal{D}, \tag{B.4d}$$

$$q_{ij,t}^{\mathrm{C}} \ge 0, \qquad \forall\,(i,j)\in\mathcal{C}, \tag{B.4e}$$

$$\underline{K}^{\mathrm{C}}\pi_{i,t} \le \pi_{j,t} \le \overline{K}^{\mathrm{C}}\pi_{i,t}, \qquad \forall\,(i,j)\in\mathcal{C}, \tag{B.4f}$$

$$\begin{aligned}
&\sum_{s\in\Psi_i^{\mathcal{S}}} q_{s,t}^{\mathrm{S}} - \sum_{j\in\Omega_i} m_{ij,t}^{\mathrm{in}} + \sum_{j\in\Omega_i} m_{ji,t}^{\mathrm{out}} \\
&- \sum_{j\in\Omega_i^{\mathrm{C}}} q_{ij,t}^{\mathrm{C}} + \sum_{j\in\Omega_i^{\mathrm{C}}} q_{ji,t}^{\mathrm{C}} - \sum_{j\in\Omega_i^{\mathrm{Cf}}} q_{ij,t}^{\mathrm{C}}\eta_c^{\mathrm{C}} - \sum_{j\in\Omega_i^{\mathrm{Cf}}} q_{ji,t}^{\mathrm{C}}\eta_c^{\mathrm{C}} \\
&- \sum_{g\in\Psi_i^{\mathcal{G}}} p_{g,t}^{\mathrm{G}}\eta_g^{\mathrm{G}} - \sum_{d\in\Psi_i^{\mathcal{D}}} (Q_{d,t}^{\mathrm{D}} - q_{d,t}^{\mathrm{O}}) = 0, \quad \forall\, i\in\mathcal{I}.
\end{aligned} \tag{B.5}$$

Constraint (B.4a) restricts gas suppliers to operate between their minimum and maximum, $\underline{Q}_s$ and $\overline{Q}_s$. Constraint (B.4b) limits the nodal gas pressure $\pi_{i,t}$ between the minimum $\underline{\Pi}_i$ and maximum $\overline{\Pi}_i$ values. Constraint (B.4c) fixes the pressures at source nodes, which are directly connected to compressors, denoted by $\mathcal{I}^{\mathrm{S}}$, to a predefined value Π_i^{S}. Constraint (B.4d) enforces gas load curtailment to be lower than or equal to the nodal gas load $Q_{d,t}^{\mathrm{D}}$. Constraint (B.4e) restricts the direction of the flow through compressors, $q_{ij,t}^{\mathrm{C}}$, whereas (B.4f) limits the pressure at the outlet of the compressor based on the minimum and maximum compression ratios, i.e., $\underline{K}^{\mathrm{C}}$ and $\overline{K}^{\mathrm{C}}$. Let Ω_i^{C} be the set of compressors starting at node i and $\Omega_i^{\mathrm{Cf}}\subseteq\Omega_i^{\mathrm{C}}$ those that draw fuel from node i. Constraint (B.5) is the nodal gas balance equation, including the gas withdrawal for producing the GFPPs power output $p_{g,t}^{\mathrm{G}}$ with the conversion efficiency η_g^{G}, and the gas withdrawal for compressor fuel consumption, calculated as the fraction η_c^{C} of the gas flow through the compressor [17].

OC.3.4. Gas flow constraints

The gas flow constraints are enforced for every pipeline $(i,j) \in \mathcal{P}$ and time step $t \in \mathcal{T}$. Binary parameters U^{QD} and U^{ST} are used to differentiate between the DY ($U^{\mathrm{ST}} = U^{\mathrm{QD}} = 1$), QD ($U^{\mathrm{ST}} = 1, U^{\mathrm{QD}} = 0$) and ST ($U^{\mathrm{ST}} = U^{\mathrm{QD}} = 0$) models. Equation (B.7) is replaced by the feasible set $\mathcal{F}^{\mathbf{S}}$ depending on the chosen solution technique presented in Section IV.

$$U^{\mathrm{ST}} \frac{\pi_{ij,t} - \pi_{ij,t-1}}{\Delta t} + \frac{c^2}{A_{ij}} \frac{m^{\mathrm{out}}_{ij,t} - m^{\mathrm{in}}_{ij,t}}{\Delta x} = 0, \tag{B.6a}$$

$$U^{\mathrm{QD}} \frac{m_{ij,t} - m_{ij,t-1}}{\Delta t} + A_{ij} \frac{\pi_{j,t} - \pi_{i,t}}{\Delta x} + \frac{\lambda_{ij} c^2}{2 D_{ij} A_{ij}} \gamma_{ij,t} = 0, \tag{B.6b}$$

$$m_{ij,t} = \frac{m^{\mathrm{in}}_{ij,t} + m^{\mathrm{out}}_{ij,t}}{2}, \tag{B.6c}$$

$$\pi_{ij,t} = \frac{\pi_{i,t} + \pi_{j,t}}{2}, \tag{B.6d}$$

$$\pi_{ij,0} = \Pi_{ij,0} \tag{B.6e}$$

$$m_{ij,0} = M_{ij,0} \tag{B.6f}$$

$$\pi_{ij,0} \leq \pi_{ij,T}, \tag{B.6g}$$

$$\underline{M}_{ij} \leq m_{ij,t} \leq \overline{M}_{ij}, \tag{B.6h}$$

$$\underline{\Gamma}_{ij} \leq \gamma_{ij,t} \leq \overline{\Gamma}_{ij}. \tag{B.6i}$$

For the first time step, i.e., $t = 1$, (B.6a) and (B.6b) require to assume the initial condition of the average pressure and flow in the pipelines at $t-1$. To determine the initial condition, we solve model DY-NLP model for 15 min time discretization twice. The first time, we assume that the system starts from a steady-state condition. This implies that, for $t = 1$, the steady-state model for (B.6a) and (B.6b) is assumed. We then solve the problem again, assuming the DY model for all time steps. The solution for the last time step of the first run is used as an initial condition for the second run. After solving the second run, the solution for the last time step is used as an initial condition for problem P-S. Note that we assume that the linepack in each pipeline must be at least restored at the end of the time horizon, i.e., $t = T$, enforced by (B.6g). Constraints (B.6h)–(B.6i) define bounds on the average flow $m_{ij,t}$ and auxiliary variable $\gamma_{ij,t}$, which can be derived as explained in Section V-A of the main paper.

Finally, the auxiliary variable $\gamma_{ij,t}$ is defined as:

$$\gamma_{ij,t} = \frac{m_{ij,t} |m_{ij,t}|}{\pi_{ij,t}}. \tag{B.7}$$

OC.4. Solution choices continued

This section contains a detailed explanation of individual parameters and additional information on some of the solution choices presented in Section IV of the main paper.

OC.4.1. Sequential linear programming

As explained in Section IV-B of the main paper, the sequential linear programming algorithm solves a series of linear optimization problems. To avoid large step sizes, the Euclidean distance between the optimal solution of two consecutive iterations is penalized using a parameter δ^k, which is updated after each iteration. We use $\delta^1 = 10^{-3}$ as an initial value. After each iteration, the penalizer is multiplied by 2, until it reaches a maximum value of $\delta^{\max} = 10^3$. The algorithm terminates when the infinity norm of the relative relaxation gap in iteration k, Φ_k^∞ is less than 10^{-12}. The penalizer and maximum violation gap are converted to per-unit by their respective bases.

OC.4.2. Mixed-integer linear relaxation

It has been proposed in [11] to choose the set of linearization points based on a uniform grid over the feasible region of the flow and pressure variables. This approach neglects the curvature of the function and may yield a low approximation accuracy at some points. Instead, we follow the same approach to deriving the polyhedral envelopes introduced in Sections IV-F and OC.4.3. To account for the modeling of the flow direction using the binary variable z and nonnegative auxiliary variables $\gamma^{+/-}$ and $m^{+/-}$, we divide the polyhedral envelops resulting from the linearization points in (C.3) into positive and negative flow direction. For envelops $u = \{1, 2, 3\}$, we replace γ and m by m^+ and γ^+. Similarly, for envelops $u = \{4, 5, 6\}$, we replace γ and m by m^- and γ^-. Additionally, we switch the signs of $\underline{M}$ to account for the nonnegativity of the flow.

The feasible region of MILP is substantially reduced compared to the PELP by including the flow directions as binary variables (see Fig. 4). To further strengthen the relaxation, we derive one additional halfspace per flow direction based on the intersection of the planes defined by $u = 1$ and $u = 4$ with nonnegativity $\gamma^+ \geq 0$ and $\gamma^- \geq 0$, respectively. Analogously to the derivation of the linearization points $\widetilde{m}^3$ and $\widetilde{m}^6$, we derive those points by fixing $\pi = \widehat{\Pi}_{ij}^+$ and $\pi = \widehat{\Pi}_{ij}^-$, respectively, and projecting the intersection point on the manifold. The flow of the resulting linearization points $u = 7$ for m^+ and $u = 8$ for m^- are then given by

$$\widetilde{m}^7 = \frac{(\sqrt{8} - 3) \cdot \overline{M}}{2 - \sqrt{8}}, \tag{C.1}$$

$$\widetilde{m}^8 = \frac{(\sqrt{8} - 3) \cdot \underline{M}}{2 - \sqrt{8}}. \tag{C.2}$$

OC.4.3. Polyhedral envelops

We generally follow the approach presented in [18] to derive the sets of linearization points $u \in \mathcal{U}$ and $o \in \mathcal{O}$, where $|\mathcal{U}| = |\mathcal{O}| = 3$. The sets $\mathcal{U}$ and $\mathcal{O}$ are used to derive under- and over-estimators, respectively. While [18] derives individual polyhedral envelops for both sides of the Weymouth equation (11), we directly derive it for the three-dimensional function in (12), by fixing the average

pipeline pressure π to a predefined value. We observed that the maximum value of γ is attained at the maximum pipeline pressure difference (see Section V-A). Therefore, we use $\widetilde{\pi}^u = \widehat{\Pi}_{ij}^+$ for $u = \{1,2,3\}$ and $\widetilde{\pi}^o = \widehat{\Pi}_{ij}^-$ for $o = \{4,5,6\}$. The corresponding points of the mass flow $\widetilde{m}^u$, for $u = 1,2,3$, and $\widetilde{m}^o$, for $o = 4,5,6$, are given by

$$\widetilde{m}^1 = (1-\sqrt{2}) \cdot \underline{M}, \qquad \widetilde{m}^4 = (1-\sqrt{2}) \cdot \overline{M} \tag{C.3}$$

$$\widetilde{m}^2 = \overline{M}, \qquad \widetilde{m}^5 = \underline{M} \tag{C.4}$$

$$\widetilde{m}^3 = \frac{-\underline{M}^2(\sqrt{8}-3) - \overline{M}^2}{\underline{M}(2-\sqrt{8}) - 2\overline{M}}, \qquad \widetilde{m}^6 = \frac{\underline{M}^2(3-\sqrt{8}) + \overline{M}^2}{\overline{M}(\sqrt{8}-2) + 2\underline{M}}. \tag{C.5}$$

We refer the interested reader to [18] for a more detailed elaboration on deriving the individual linearization points.

OC.4.4. Piecewise linear approximation

It has been frequently proposed in the literature to use a one-dimensional piecewise linearization of both sides of the Weymouth equation (11) based on a predefined set of fixed points, see, e.g., [8,10]. Similarly, although more complex, a two-dimensional piecewise linearization of (12) can be derived. Here, we adopt the logarithmic disaggregated convex combination model presented in [19], as it is computationally preferable to other piecewise linearization methods [20]. We term the resulting model **P**-PWL. The solution to this model will generally inhibit an approximation error, which, similar to the relaxation-based models, implies a violation of the gas flow physics. However, the magnitude of the error is usually smaller and controllable by the number of linearization points. Even with the minimum number of linearization segments, we could not solve the resulting problem for a small case study. Therefore, we do not consider this modeling approach further and refer the interesting reader to [20] to review existing approaches, which have also been applied to gas flow modeling.

OC.5. Applying per unit conversion

Due to the slow dynamics of gas flows in pipelines, the OPGF is numerically challenging. Taking a look at the conservation of momentum constraint (5) in the main paper, assuming a pipeline diameter $D = 1\,\text{m}$ and space discretization of $\Delta x = 50\,\text{km}$, the coefficients in front of the pressure drop and friction factor are around 10^{-4} and 10^4, respectively. Similar to power systems analysis, those numerical issues can be tackled by applying a per-unit conversion, which transforms all variables and parameters into dimensionless quantities without distorting the underlying relations and the structure of the problem. This is done by defining interdependent base values according to the physical dimensions of the variables and parameters.

For the PDEs governing the gas flow, there are three degrees of freedom in choosing the bases. We decide to choose a base for the pressure Π^{B} in Pa, the spatial dimension D^{B} in m and time T^{B} in s. From those, the bases for the cross-sectional area A^{B} in m^2, the speed of sound in gas C^{B} in m/s, and the one for the mass flow M^{B} in kg/s are derived based on their respective units:

$$A^{\mathrm{B}} = (D^{\mathrm{B}})^2, \quad C^{\mathrm{B}} = D^{\mathrm{B}}/T^{\mathrm{B}}, \quad M^{\mathrm{B}} = D^{\mathrm{B}}\Pi^{\mathrm{B}}T^{\mathrm{B}}. \tag{C.6}$$

The bases for the auxiliary variable γ, Γ^{B} is derived based on Equation (12) in the main paper as:

$$\Gamma^{\mathrm{B}} = \frac{(M^{\mathrm{B}})^2}{\Pi^{\mathrm{B}}}. \tag{C.7}$$

All model parameters are then divided by their respective bases. The solution to the original problem can be recovered by multiplying the optimal solutions of the decision variables by their respective bases. As long as the bases are derived according to the physical dimensions, the problems with and without per-unit conversion are mathematically equivalent.

GFPPs couple the power and gas systems based on their gas-to-power conversion efficiency η in MW s/kg. Using the base power S^{B} of the power system, the base value for the efficiency can be calculated as $\eta^{\mathrm{B}} = M^{\mathrm{B}}/S^{\mathrm{B}}$. This makes the proposed per-unit conversion for the gas system appealing to integrated power and gas system studies, as it is widely established in power systems analysis.

To apply the per-unit conversion to different gas networks and discretizations and avoid a manual tuning of base values, we solve a small unconstrained minimization problem to find the optimal bases for spatial and time dimensions D^{B} and T^{B}, respectively, which minimizes the Euclidean distance between the magnitudes of the parameters of the conservation of mass and momentum constraints (4)–(5) and a center Z:

$$\begin{aligned}\min_{D^{\mathrm{B}},T^{\mathrm{B}}} &(\log_{10}\left(\frac{T^{\mathrm{B}}}{\Delta t}\right) - Z)^2 + (\log_{10}\left(\frac{(c\cdot T^{\mathrm{B}})^2 D^{\mathrm{B}}}{\Delta x}\right) - Z)^2 + \\ &(\log_{10}\left(\frac{T^{\mathrm{B}}}{\Delta t}\right) - Z)^2 + (\log_{10}\left(\frac{1}{D^{\mathrm{B}}\Delta x}\right) - Z)^2 + (\log_{10}\left(\frac{\widetilde{\lambda}(c\cdot T^{\mathrm{B}})^2 D^{\mathrm{B}}}{2\widetilde{D}^3\Delta x}\right) - Z)^2,\end{aligned} \tag{C.8}$$

where Δx and Δt are the chosen space and time discretization, c is the speed of sound in the gas, and $\widetilde{\lambda}$ and $\widetilde{D}$ are the friction factor and the pipeline diameter that reflect the network topology. We choose the average friction factor and smallest pipeline diameter observed in the network. Based on feasibility tolerances of 10^{-4}, we choose $Z = 1$.

For high-pressure gas transmission networks, we choose $\Pi^{\mathrm{B}} = 0.5\,\mathrm{MPa}$. Based on problem (C.8), we find values of around $D^{\mathrm{B}} = 1\cdot 10^{-7}$ and $D^{\mathrm{T}} = 2\cdot 10^{3}$ for a discretization of $\Delta t = 1\,\mathrm{h}$ and $D^{\mathrm{B}} = 2.5\cdot 10^{-7}$ and $D^{\mathrm{T}} = 1\cdot 10^{3}$ for $\Delta t = 15\,\mathrm{min}$. The remaining base values can be calculated as

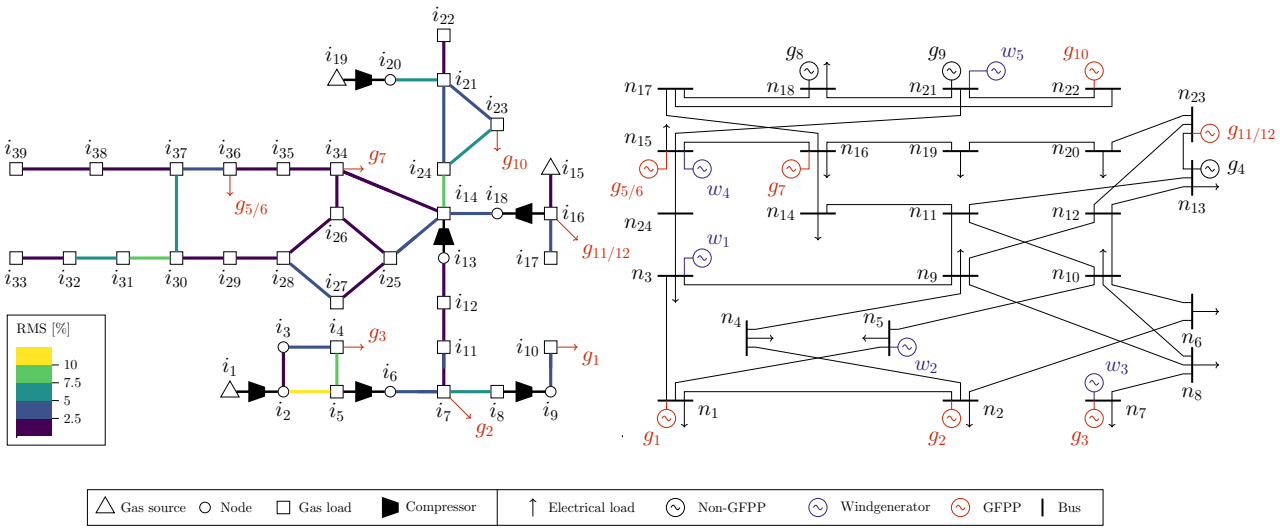

Figure OC.5 **Case study B: GasLib 40-node gas network connected to 24-bus IEEE RTS system. Innode 3 and pipelines 33 and 39 are removed from the gas network to avoid circular flows arising from the neglect of compressor states. Pipeline colors indicate the value of the root mean squared (RMS) relaxation gap of each pipeline for the optimal solution of model** DY-PELP**.**

explained above. Note that the range of the parameters, i.e., the optimal value of problem (C.8), decreases with a finer discretization, such that the numerical issues are reduced.

Finally, we transform all the cost parameters of the objective function using a cost base of 1000 €.

OC.6. Case Study B: Large-scale integrated power and gas system

To analyze the impact of the considered solution choices on a realistic large-scale integrated power and gas system, we consider Case Study B, which is a modified version of the GasLib 40-node gas network [21] connected to a modification of the 24-bus IEEE RTS power system in [22]. A schematic diagram of the integrated system is shown in Figure OC.5.

To avoid circular gas flows arising from the neglection of operational states of the compressors, innode 3 and pipelines 33 and 39 have been removed from the gas network. We set a pressure range of 31 −81 bar for all nodes. The pressure at source nodes before compressors is fixed such that the maximum nodal pressure at the compressor outlet is met at full compression. Given a maximum compression ratio of 1.5 , this is around 54 bar. We use the same profiles shown in Fig. 2 of the main paper for all electrical loads, gas loads, and wind farms, varying their peak load and installed capacity, respectively. The data can be found in the GitHub repository [7]. We consider the DY model only and apply a time and space discretization of 15 min and 50 km, respectively. Except for solution choices NLP, SLP, and PELP, no other method was able to solve the OPGF problem within 24 h.

The different colors of the pipelines in Figure OC.5 illustrate each pipeline's root mean squared (RMS) relaxation gap. This is done by calculating Φ^{RMS} according to Equation (23) for each pipeline (i, j) using the stacked relative relaxation gaps $\mathbf{\Phi}_{ij}$ and without normalizing by the square-root of the total number of pipelines. Generally, it can be observed that the relaxation gap is, on average, higher around junctions. Assuming, e.g., gas flows from a junction into two pipelines with the same pressure gradient. Then, the relaxation gap can be utilized to have a proportionally lower flow on one of the connected branches. For solution choices MILP and PELP, a flow over proportionally high compared to the pressure gradient could also be feasible. However, since the pressure ranges are usually nonbinding, this rarely happens, as a larger pressure gradient could be chosen.

References

[1] M. V. Lurie, *Modeling of oil product and gas pipeline transportation.* Wiley, 2009.

[2] E. S. Menon, *Gas pipeline hydraulics.* Taylor & Francis Group, 2005.

[3] C. Liu, M. Shahidehpour, and J. Wang, "Coordinated scheduling of electricity and natural gas infrastructures with a transient model for natural gas flow," *Chaos: An Interdisciplinary Journal of Nonlinear Science*, vol. 21, no. 2, p. 025102, 2011.

[4] C. M. Correa-Posada and P. Sánchez-Martín, "Gas network optimization: A comparison of piecewise linear models," *Optimization Online*, pp. 1–24, 2014. [Online]. Available: https://optimization-online.org/?p=13086

[5] W. Wei and J. Wang, *Modeling and optimization of interdependent energy infrastructures.* Springer, 2020.

[6] C. O'Malley, "Coordination of gas-electric networks: Modeling, optimization and uncertainty," Ph.D. dissertation, ETH Zurich, 2021.

[7] E. Raheli, Y. Werner, and J. Kazempour, "Flexibility of integrated power and gas systems: Modeling and solution choices matter – Online companion," 2023, https://github.com/ELMA-Github/OptimalPowerGasFlowChoices.

[8] C. M. Correa-Posada and P. Sánchez-Martín, "Integrated power and natural gas model for energy adequacy in short-term operation," *IEEE Trans. Power Syst.*, vol. 30, no. 6, pp. 3347–3355, 2015.

[9] Q. Zeng, B. Zhang, J. Fang, and Z. Chen, "A bi-level programming for multistage co-expansion planning of the integrated gas and electricity system," *Appl. Energy*, vol. 200, pp. 192–203, 2017.

[10] C. He, L. Wu, T. Liu, and M. Shahidehpour, "Robust co-optimization scheduling of electricity and natural gas systems via admm," *IEEE Trans. Sustain. Energy*, vol. 8, no. 2, pp. 658–670, 2017.

[11] C. Ordoudis, P. Pinson, and J. M. Morales, "An integrated market for electricity and natural gas systems with stochastic power producers," *Eur. J. Oper. Res.*, vol. 272, no. 2, pp. 642–654, 2019.

[12] M. Qadrdan, J. Wu, N. Jenkins, and J. Ekanayake, "Operating strategies for a GB integrated gas and electricity network considering the uncertainty in wind power forecasts," *IEEE Trans. Sustain. Energy*, vol. 5, no. 1, pp. 128–138, 2014.

[13] J. F. Helgaker, "Modeling transient flow in long distance offshore natural gas pipelines," Ph.D. dissertation, Norwegian University of Science and Technology, 2013.

[14] F. Hennings, "Large-scale empirical study on the momentum equation's inertia term," *J. Nat. Gas Sci. Eng.*, vol. 95, p. 104153, 2021.

[15] A. Osiadacz, "Simulation of transient gas flows in networks," *Int. J. Numer. Methods Fluids*, vol. 4, no. 1, pp. 13–24, 1984.

[16] A. Herrán-González, J. M. De La Cruz, B. De Andrés-Toro, and J. L. Risco-Martín, "Modeling and simulation of a gas distribution pipeline network," *Appl. Math. Model.*, vol. 33, no. 3, pp. 1584–1600, 2009.

[17] S. Wu, R. Ríos-Mercado, E. Boyd, and L. Scott, "Model relaxations for the fuel cost minimization of steady-state gas pipeline networks," *Math. Comput. Model.*, vol. 31, no. 2, pp. 197–220, 2000.

[18] S. Mhanna, I. Saedi, and P. Mancarella, "Iterative LP-based methods for the multiperiod optimal electricity and gas flow problem," *IEEE Trans. Power Syst.*, vol. 37, no. 1, pp. 153–166, Jan. 2022.

[19] J. P. Vielma and G. L. Nemhauser, "Modeling disjunctive constraints with a logarithmic number of binary variables and constraints," *Math. Program.*, vol. 128, no. 1-2, pp. 49–72, Jul. 2009.

[20] B. Geißler, A. Martin, A. Morsi, and L. Schewe, "Using piecewise linear functions for solving MINLPs," in *Mixed Integer Nonlinear Programming.* Springer New York, Nov. 2011, pp. 287–314.

[21] M. Schmidt, D. Aßmann, R. Burlacu, J. Humpola, I. Joormann, N. Kanelakis, T. Koch, D. Oucherif, M. E. Pfetsch, L. Schewe, R. Schwarz, and M. Sirvent, "GasLib – A Library of Gas Network Instances," *Data*, vol. 2, no. 4, p. article 40, 2017.

[22] C. Ordoudis, P. Pinson, J. M. Morales, and M. Zugno, "An updated version of the IEEE RTS 24-bus system for electricity market and power system operation studies," *Technical University of Denmark*, 2016, https://orbit.dtu.dk/en/publications/an-updated-version-of-the-ieee-rts-24-bus-system-for-electricity-.